Quantification of the Level of Samarium/Barium Substitution in the Ag-$Sm_{1+x}Ba_{2-x}Cu_3O_{7-\delta}$ System

Wen Zhao[*1], Yunhua Shi[*], Difan Zhou[*], Anthony R. Dennis[*], David A. Cardwell[*]

[*] *Bulk Superconductivity Group, Department of Engineering, University of Cambridge, United Kingdom*

[1] *Corresponding author E-mail: zhaowen0910@hotmail.co.jp Contact No.: +86 13909962397*

Abstract

The high-temperature $SmBa_2Cu_3O_{7-\delta}$ (Sm-123) superconducting system, which is characterised by a high critical transition temperature (T_c) and a high critical current density (J_c), suffers severely from the effects of Sm/Ba substitution in the superconducting Sm-123 phase matrix, and especially so for large, single grains grown in air, resulting in a significant variation in T_c at different positions within a single grain. As a result, the suppression of Sm/Ba substitution in the $Sm_{1+x}Ba_{2-x}Cu_3O_{7-\delta}$ phase matrix (SmBCO, where x represents the Sm/Ba substitution level in the SmBCO system) is critical to achieving good superconducting properties in this material. Here we report the use of Electron Probe Micro-Analysis (EPMA) to investigate, adjust and optimise the composition of mechanically-stabilised standard Ag-SmBCO bulk single grains. We show that the substitution levels within these samples changes linearly within increasing distance from the vicinity of a single crystal seed used to nucleate the single grain growth process. In addition, we identify a constant value of x of – 0.080 for the composition-adjusted Ag-SmBCO bulk single grain. This is the first time that the quantification of the Sm/Ba substitution level in the SmBCO system has been measured accurately and directly using EPMA, and

suggests clearly that the Sm/Ba substitution can be suppressed effectively in air. This research will provide significant insight into the development of a process to suppress Sm/Ba substitution even further in superconducting SmBCO single grains in the future.

Keywords: Superconductor, Perovskites, Rare-earth, Electron Probe Micro-Analysis (EPMA)

1. Introduction

$SmBa_2Cu_3O_{7-\delta}$ (Sm-123, or SmBCO) is a member of the $(RE)Ba_2Cu_3O_{7-\delta}$ (RE-123) family (where RE is rare earth element or Y) of high-temperature superconductors (HTS). SmBCO fabricated in the form of large, single grains by melt processing has significant potential for use in practical applications due to its high critical transition temperature (T_c), high critical current density (J_c), the so-called 'peak effect' characteristic present in its magnetic hysteresis (***M-H***) behaviour in high applied magnetic field and high irreversibility field. SmBCO bulk superconductors are capable of supporting macroscopic currents at temperatures above the boiling point of liquid nitrogen (77 K), and can, therefore, be used potentially in a variety of high field, quasi-permanent magnet applications such as magnetic bearings [1] and flywheel energy storage systems [2]. It is necessary to process SmBCO materials in the form of large, single grains and avoid the presence of grain boundaries, however, if the SmBCO bulk superconductor is to carry large currents on the length scale of the sample, which is essential for the generation of magnetic fields that are much larger than those produced by conventional permanent magnet materials [3]. The growth of

superconducting (RE)BCO single grains has been developed systematically over the past 30 years, and processes to achieve the stable growth of large SmBCO single grains has been achieved. In general, however, the processing conditions required for SmBCO bulk superconductors are more complicated than those for $YBa_2Cu_3O_{7-\delta}$ (YBCO), which has been investigated more extensively, due primarily to the high melting temperature of the precursor powders, rapid growth rate, which is difficult to control, and the need to process SmBCO under reduced oxygen partial pressure in order to inhibit the substitution of samarium (Sm) on the barium (Ba) site in the superconducting Sm-123 phase matrix [4]. Reducing the substitution level of Ba by Sm in the SmBCO system in a practical processing environment represents a particular challenge due primarily to the severity of this effect in air, which leads directly to vastly inferior superconducting properties compared even with the properties of YBCO single grains. As a result, extensive research performed worldwide on the suppression of Sm/Ba substitution in SmBCO has identified that the effects of substitution can be reduced by the addition of a small amount of BaO_2 or $BaCuO_2$ to the SmBCO precursor powders prior to melt processing [5]. Although the Sm/Ba substitution can be suppressed to some extent by this technique, the inherent inhomogeneity of the superconducting SmBCO single grains grown subsequently in air limits the effectiveness of this approach, since different amounts of the additional Ba are required throughout the SmBCO single grain growth process to uniformly suppress the extent of Sm/Ba substitution. Furthermore, Sm/Ba substitution occurs in Sm-123 matrix containing embedded, discrete Sm_2BaCuO_5 (Sm-211) inclusions

throughout the entire cross section of the sample. As a result, the detectable microscopic length over which the local Sm-123 composition can be measured reliably (i.e. without impingement of Sm-211) is confined, roughly, to 2–10 μm. Beyond that, the Sm/Ba substitution levels at different positions within the single grain are extremely difficult to detect, which presents a significant challenge to energy dispersive x-ray spectrometry (EDX), which is the characterisation technique used most commonly for the characterisation of chemical composition in refractory metal oxides. This is another reason why the precise measurement of the Sm/Ba substitution level in the SmBCO system is rarely possible.

The distribution and extent of Sm/Ba substitution in the SmBCO system has yet to be studied systematically, despite its fundamental influence on the superconducting properties of SmBCO single grains. In this paper, we report for the first time the precise quantification of the Sm/Ba substitution level in the SmBCO system using an Electron Probe Micro-analyser (EMPA). Single grain Ag-SmBCO bulk samples grown by top seeded melt growth (TSMG) with and without the presence of a $YBa_2Cu_3O_{7-\delta}$ (Y-123) layer, added in order to modify the composition to confirm the effectiveness of the method, were measured and analysed systematically as part of this study. The substitution level within the bulk SmBCO samples has been quantified extensively from the top surface to the bottom of the samples, discussed in detail and correlated with the results of their measured superconducting properties, demonstrating unequivocally that EPMA is an effective method for identifying accurately the Sm/Ba substitution level in the SmBCO system. Finally, the addition of

a layer of Y-123 at the bottom of the pressed SMBCO pre-forms prior to melt processing leads directly to a more uniform matrix composition in the fully processed SmBCO single grains, which, in turn, results in greater control of the extent of Sm/Ba substitution.

2. Experimental

2.1 Production of Ag-SmBCO Single Grains in Air with and without a Y-123 Layer

Commercial Sm-123 (TOSHIMA, average particle size 2-3 μm) and Sm-211 (TOSHIMA, average particle size 1-2 μm) precursor powders in a weight ratio of 3:1, together with 2 wt. % BaO_2 (ALDRICH, purity 95 %) to suppress Sm/Ba substitution [5], 1 wt. % CeO_2 (Alfa Aesar, purity 99.9%), to reduce the coarsening of the Sm-211 second phase particles [6] and 10 wt. % of Ag_2O (Alfa Aesar, purity 99+ %, metal basis), to improve the mechanical strength and cracking resistance [7], were mixed thoroughly using a mortar and pestle to yield a net composition of (75 wt. % Sm-123 + 25 wt. % Sm-211) + 2 wt. % BaO_2 + 1 wt. % CeO_2 + 10 wt. % Ag_2O (abbreviated to Ag-SmBCO). The resulting powder was pressed uniaxially into a dark green pellet of diameter 32 mm and thickness 16 mm, which yielded final, as-processed dimensions of 25 mm diameter and 13 mm thickness after a shrinkage about 80 % during melt growth. 6 g of commercially available Y-123 (TOSHIMA, average particle size 2-3 μm) and 2 g of Yb_2O_3 (American Elements, purity 99%) to provide an inert layer, were pressed to form a combined supporting pellet using the same size die as the bulk pre-forms to replace the yttrium-stabilised ZrO_2 rods used

commonly to support (RE)BCO samples during melt processing. A generic seed crystal [8] [9] was used to nucleate and grow the required grain orientation with an associated buffer layer, the preparation and properties of which are reported elsewhere [10]. At high temperatures, the seed melts partially at its interface with the SmBCO precursor pellet, so contact with the bulk pre-form may lead to contamination of the seeding material and consequently lower the melting temperature of the seed, which results in dissolving and/or the deterioration of the seed. A minimum thickness of 100 μm is required, therefore, for the seed crystal to retain its integrity [11] to avoid such a problem. To further avert the potential of the contaminations from the seed, a buffer layer is additionally added between the generic seed and the Ag-SmBCO perform in this research. The seed, the buffer layer and the Ag-SmBCO pre-form (with and without Y-123 and Yb_2O_3 layers) were aligned before melt processing to yield the required orientation of the single grain, as illustrated schematically in Figure 1 (a). The arrangement was placed on an alumina plate in a box furnace prior to top seeded melt growth (TSMG) using the heating profile shown schematically in Figure 1 (b). The TSMG process is based on a peritectic solidification reaction that occurs at the peritectic temperature, T_p (1045 ℃ for the starting powder composition in Ag-SmBCO system in this paper), during which solid Sm-123 is formed from solid Sm-211, a Ba-Cu-O based liquid phase (L) and oxygen gas (G) [12];

$$\text{Sm-211} + Ba_3Cu_5O_{6.72}\ (L) + 0.42O_2\ (G) \rightarrow 2\ \text{Sm-123} \qquad (1\text{-}1)$$

The Ag-SmBCO single grain growth process involved ramping the temperature initially to 1070 ℃, holding at this temperature for 20 minutes to allow thorough decomposition of the precursor powders and cooling the furnace to 1037 ℃ at a rate of 50 ℃ h^{-1}, at which the growth of the bulk single grain begins. The cooling rate was then decreased to 1 ℃ h^{-1} at this temperature, then further to 0.5 ℃ h^{-1} over the temperature range between 1024 ℃ and 1010 ℃ and then slow cooled at a rate of 0.3 ℃ h^{-1} to 1004 ℃, to complete growth of the single grain. Finally, the sample was furnace-cooled to room temperature.

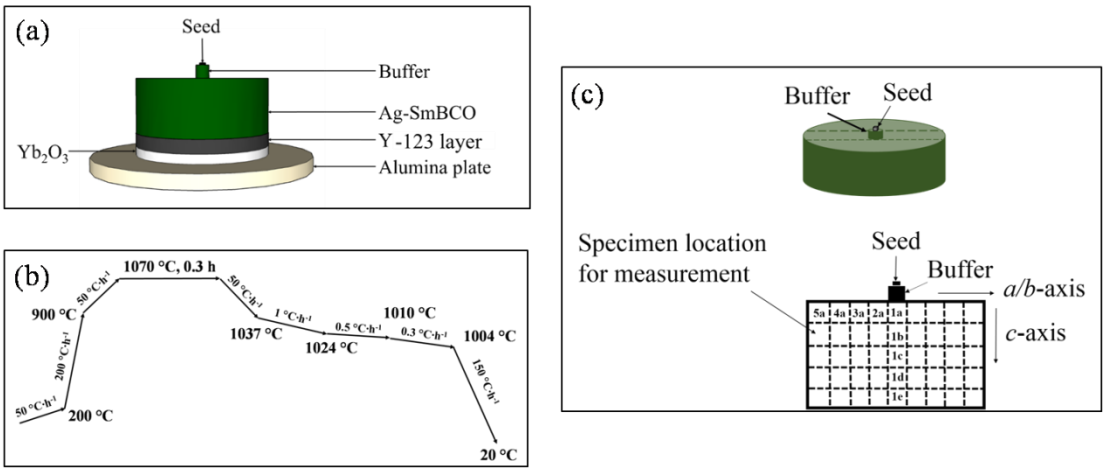

Figure 1 (a) Schematic illustration of an Ag-SmBCO bulk pre-form with a Y-123 layer prior to TSMG, (b) Schematic illustration of the heating profile used in the TSMG process for the Ag-SmBCO single grains processed with and without a Y-123 layer and (c) Schematic illustration of the sub-sample scheme for the preparation of the SQUID specimens.

The as-grown samples were oxygenated subsequently at 360 ℃ for fourteen days to drive the non-superconducting, tetragonal Sm-123 phase to the desired orthorhombic, superconducting phase.

2.2 Characterisation

2.2.1 Superconducting Properties, T_c and J_c, of Ag-SmBCO Single Grains Processed with and without a Y-123 Layer

The spatial variation in T_c and J_c throughout the single grain bulk samples was measured using a Superconducting Quantum Interference Device (SQUID) MPMS XL magnetometer. The MPMS XL SQUID system is capable of measuring very small magnetic moments with a nominal sensitivity of 1×10^{-11} A m^2. The range of the measurement temperature was from 1.9 K to 300 K with a magnetic field induction of ± 7 T.

The samples to be measured were cut into slices across their centre, with each slice being cut further into smaller specimens of size approximately 1.5 mm × 2.0 mm × 1.2 mm at different positions within the bulk single grain, as shown schematically in Figure 1 (c). A field of 0.002 T was applied to the samples after zero-field-cooling prior to the measurement of T_c. The extended Bean critical state model [13] was used to calculate J_c at 77 K from the measured magnetic hysteresis loops of the sub-specimens (i.e. from the measured ***M*-*H*** loops).

2.2.2 Optical Microscopy of Ag-SmBCO Single Grains Processed with and without a Y-123 Layer

Optical microscopy was used to examine the size and distribution of Sm-211 particles in the as-grown Ag-SmBCO single grains with and without a Y-123 layer along *c*-axis. The as-prepared superconducting pellets were cut into two halves along the *c*-axis through the seed and the exposed cross-section was polished sequentially using

120, 220, 320, 800, 1000, 1200 and 2400 grit SiC papers. Further polishing was achieved by using 3 μm and 1 μm diamond spray. A Nikon Eclipse ME600 optical microscope was used to observe the microstructures of the exposed cross-sections.

2.2.3 Chemical Composition Analysis of Ag-SmBCO Bulk Single Grains with and without a Y-123 Layer

The $SmBa_2Cu_3O_{7-\delta}$ (δ = 0–1), or Sm-123, superconducting phase is characterised crystallographically by a distorted oxygen-deficient perovskite structure, as shown in Figure 2. The stacking axis in this structure coincides with the longest unit cell parameter, denoted as the *c*-axis, with the plane perpendicular to the *c*-axis being labelled as the *a/b*-plane [14]. The oxygen atoms at the top and bottom faces in the Sm-123 crystallographic structure are the least stable energetically and may be lost most readily from the unit cell. The value of δ in the $SmBa_2Cu_3O_{7-\delta}$ phase changes between 0 and 1 with the loss of these oxygen atoms. In addition, a change in structure from orthorhombic ($a \neq b$) to tetragonal ($a = b$) occurs when the number of oxygen atoms decreases from 7 to 6. Instead of forming a stoichiometric $SmBa_2Cu_3O_{7-\delta}$ phase compound, however, a solid solution of $Sm_{1+x}Ba_{2-x}Cu_3O_{7-\delta}$ (Sm-123ss) is formed in within the base Sm-123 phase, corresponding to atomic substitution of the Ba site by Sm (x is defined as the Sm/Ba substitution level in the SmBCO system in this paper). This leads to a depression in T_c, and can be explained, at least in part, in terms of the decrease of the carrier density associated with the trivalent Sm ion replacing the divalent Ba ion. As a result, structural change is associated with disorder in the CuO chain site, which is accompanied by the

introduction of extra oxygen ions at anti-chain sites to maintain the charge balance and stoichiometry [15].

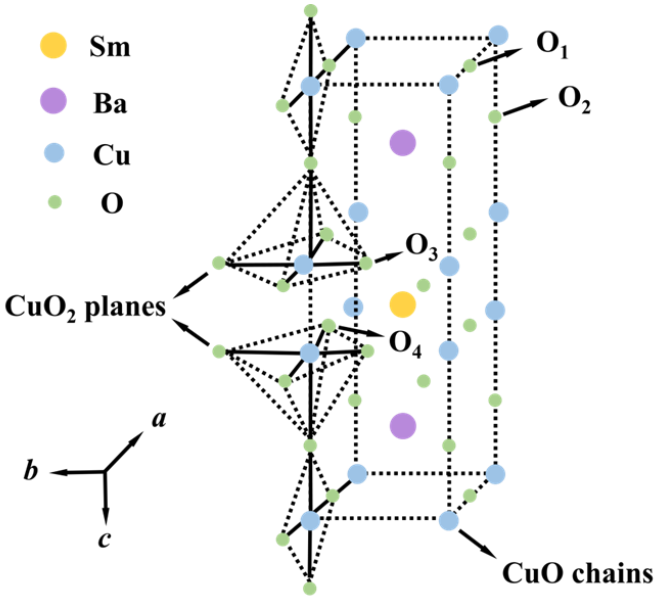

Figure 2 Oxygen-deficient perovskite structure of the superconducting Sm-123 phase [6].

Detailed analysis of the chemical composition of the $Sm_{1+x}Ba_{2-x}Cu_yO_z$ phase matrix of Ag-SmBCO single grains prepared with and without a Y-123 layer with increasing position from the seed along the *c*-axis was carried out using an Electron Probe Micro-Analyser (EPMA, CAMECA SX 100). An electron beam of a size of 1 μm was focused onto Sm-211 free regions with increasing distance from the vicinity of the seed along the *c*-axis of each sample at all positions from the top to the bottom of the bulk single grain. Cu, $BaTiSi_3O_9$ and SmF_3 were used as standard reference compositions for the Sm, Ba and Cu elements in the EPMA analysis in order to minimize errors in determining the $Sm_{1+x}Ba_{2-x}Cu_yO_z$ local phase composition within the bulk single grains.

3. Results and Discussion

3.1 Superconducting Properties: T_c and J_c

The substitution of Ba by Sm in the SmBCO system is responsible partly for the appearance of the so-called secondary "fishtail" peak effect in the ***M-H***. This peak effect is believed to originate from the formation of local, oxygen-deficient regions in the Sm-123 microstructure, which have been attributed to effective field-induced pinning. When exposed to an external magnetic field, the Sm-123ss in the lattice may disturb the superconducting order parameter at the nanoscale level, therefore providing a pinning force to the motion of magnetic flux [16].

The inherent relationship between the Sm/Ba substitution level and the superconducting properties of the Ag-SmBCO single grains influences directly the distribution of the superconducting properties (T_c and J_c) within an Ag-SmBCO superconducting bulk single grain, and motivates the need for EPMA analysis. A photograph of an Ag-SmBCO bulk single grain of diameter 25 mm is shown in Figure 3 (a). It can be seen that this fully melt processed sample exhibits characteristic four-fold growth sector boundaries on its top surface, indicating the successful growth of an Ag-SmBCO superconducting bulk single grain.

The superconducting properties, T_c and J_c, of the sample shown in Figure 3 (a) along the crystallographic *c*-axis are presented in Figure 3 (b) and (c), respectively.

It can be concluded from the measurements of T_c and transition width, ΔT_c (the difference between the onset and offset T_c) shown in Figure 3 (b) that the variation in

superconducting properties is significant for the Ag-SmBCO single grain fabricated without a Y-123 layer. Higher T_c (93 K) and narrower ΔT_c are observed in sub-specimens at positions near the top surface of this sample and at locations benneath the site of the seed, such as 1b and 1c. T_c at position 1d for specimens further away from the seed, for example, decreases to 92.5 K and even further to 92.0 K at position 1e. The sub-specimens exhibit wider ΔT_c at both these more distant positions.

J_c calculated using the extended Bean critical state model [13], shown in Figure 3 (c), exhibits similar spatial variation as T_c. J_c for the sample fabricated without a Y-123 layer exhibits an inhomogeneous distribution throughout the parent single grain, which is not favourable for trapping magnetic field, such as that required for macro-scale practical applications [17]. In general, the Ag-SmBCO sub-specimens at positions 1b and 1c exhibit a more pronounced peak effect and higher irreversibility field than at positions 1d and 1e. In summary, J_c exhibits a smaller irreversibility field and various secondary peak effects with different values of J_{c0}, which is J_c at zero field in this paper, over the entire cross-section of the sample.

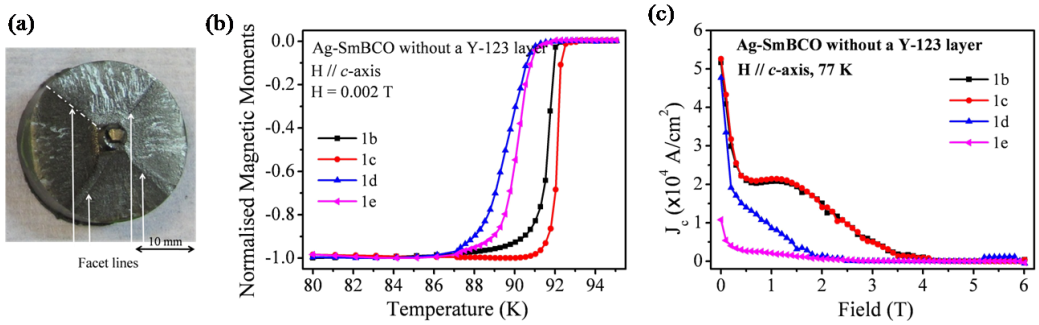

Figure 3 (a) A photograph of the top surface of a Ag-SmBCO single grain sample melt processed without a Y-123 layer, (b) normalised magnetic moment as a function of temperature and (c) critical current density, J_c, as a function of magnetic field for Ag-SmBCO processed without a Y-123 layer. The locations of the specimens within the parent single grain correspond to the positions illustrated in Figure 1 (c).

EMPA measurements of the composition distribution along the *c*-axis correlate well with the results of SQUID magnetometry, as shown in Figure 4 (a). The green solid lines in Figure 4 (a) are included to highlight the trend of the data. It can be seen that the amount of Sm decreases with increasing distance from the vicinity of the seed for the sample fabricated without a Y-123 layer and as the amount of Ba increases, indicating more severe Sm/Ba substitution effects towards the bottom of the bulk single grain, which is consistent with the T_c and J_c measurements. Interestingly, Iida *et al.* [18] reported on the substitution of Nd on Ba site in $NdBa_2Cu_3O_{7-\delta}$ (NdBCO), another member from the RE-123 superconducting family and reached to a conclusion that the substitution levels of Nd on the Ba site gradually decreased with increasing the distance from a seed. We could have expected a similar tendency of the Sm/Ba substitution in SmBCO bulks considering the resemblance between SmBCO and NdBCO systems. However, it was found that the range of Nd–Ba solid solution decreased with increasing the distance from the seed, which is not the case in this reserach and thus leading to an inconsistent result. In addition, the substitution levels in NdBCO and SmBCO systems are sensitive to the amount of Ba in precursor powders. Firstly, it is difficult to confirm the absolute amount of Nd(Sm) and Ba in

commercial precursor powders; secondly, in this paper, extra 2 wt. % BaO_2 powders were added into the precursor powders, which further complicates the situation and may lead to different conclusions. This, at the same time, manifests the complexity of the RE-123 superconducting family; the similarities between different systems may lead to opposite behaviours.

3.2 Chemical Composition of the $Sm_{1+x}Ba_{2-x}Cu_yO_z$ Matrix in Ag-SmBCO Processed without a Y-123 Layer

EPMA measurements were used to further estimate the extent of Sm/Ba substitution within the Ag-SmBCO bulk single grains. Instead of measuring directly the atomic ratio of oxygen in $Sm_{1+x}Ba_{2-x}Cu_yO_z$, the amount of oxygen in the sample was estimated, and found to be effectively constant, by data processing software on data acquired for Sm, Ba and Cu based on the stoichiometric composition of the SmBCO single grain. Figure 4 (b) shows the atomic ratios of Sm, Ba and Cu along the *c*-axis with increasing distance from the seed. The figure shows that the content of Cu is also effectively constant along the *c*-axis. Therefore, when calculating the value of x in the $Sm_{1+x}Ba_{2-x}Cu_yO_z$ superconducting phase formula, it is only necessary to consider specifically the variation in concentration of Sm and Ba elements, with the amounts of Cu and O assumed to be constant.

The average value of x in $Sm_{1+x}Ba_{2-x}Cu_yO_z$ was estimated from the data shown in Figure 4 (c). A relatively large variation in this parameter is observed in Ag-SmBCO fabricated without a Y-123 layer. The value of x in $Sm_{1+x}Ba_{2-x}Cu_3O_{7-\delta}$ can be determined reliably since the data are reasonably constant and their variation is within

1 mol. %, which is well within the error of EPMA. The results show that the concentrations of Sm and Ba within this sample change linearly with increasing position away from the seed, which suggests that the value of x follows a similar trend. This is the first time that the substitution level of Sm/Ba in Ag-SmBCO system is been quantified with this degree of accuracy, and explains why the Sm/Ba substitution is difficult to suppress, since the Sm/Ba substitution levels vary significantly at different positions in the bulk single grain.

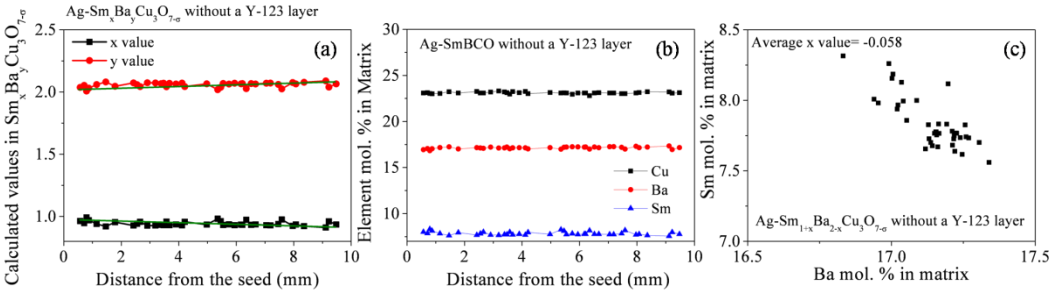

Figure 4 (a) Calculated values of x and y in Ag-Sm-123 processed without a Y-123 layer with increasing distance from the seed along the *c*-axis, (b) molar ratios of the elements in the matrix of Ag-SmBCO fabricated without a Y-123 layer with increasing distance from the seed along the *c*-axis and (c) the concentration distribution of Sm and Ba in Ag-SmBCO fabricated without a Y-123 layer.

3.3 Ag-SmBCO Samples Processed with a Y-123 Layer

To further confirm the effectiveness and accuracy of the EMPA measurements on quantifying the Sm/Ba substitution level in the Ag-SmBCO system, bulk samples were prepared with an additional Y-123 layer beneath the pre-form to enrich the liquid phase composition and, therefore, to adjust the Ag-SmBCO composition during

the TSMG process [19]. Zhou *et al.* [19] have performed extensive research on the function of the Y-123 layer on the growth and superconducting properties of $GdBa_2Cu_3O_{7-\delta}$ (GdBCO) bulk single grains. Considering the similarities between the GdBCO and SmBCO systems, therefore, it is reasonable to apply this technique to the melt processing of SmBCO. The presence of a homogeneous dispersion of Sm_2BaCuO_5 (Sm-211) particles maintains a mass balance during melt processing, which, ultimately, minimizes the residue of unreacted liquid phase and avoids the accumulation of Sm-211 particles due to particle pushing effects [19]. Leakage of liquid phase from the sample during melt growth becomes negligible, even up to 1090 ˚C, by employing Y-123 powder as a liquid source, which limits the extent to which the concentration of Sm-211 particles can vary during the growth process. More importantly, the presence of the Y-123 layer yields a more uniform distribution of Sm-211 particles in the fully processed sample, rather than an accumulation of Sm-211 particles at the growth sector boundaries, which is often observed in the single grain microstructure.

The formation of high density sub-grain boundaries is largely inhibited by providing a liquid rich environment, which, consequently, should yield a more homogeneous chemical composition throughout the sample. The top surface of the as-grown SmBCO single grain, shown in Figure 5 (a), exhibits four clear facet lines (i.e. where the four *a/b*-growth sectors intersect), indicating a homogeneous growth process, as described above.

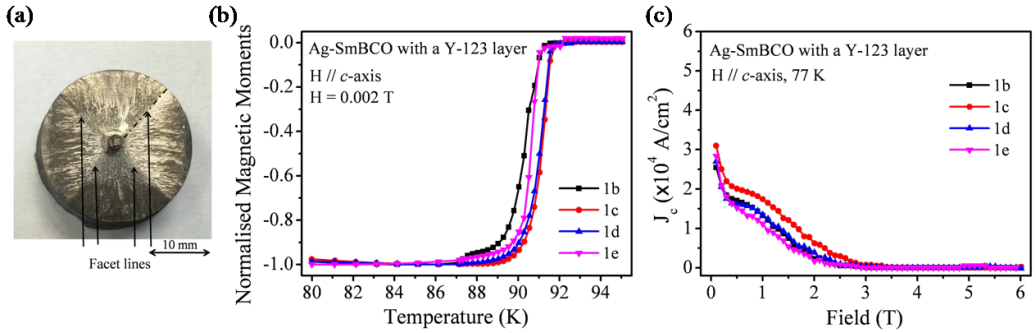

Figure 5 (a) Photograph of the top view of the Ag-SmBCO single grain sample processed with a Y-123 layer, (b) normalised magnetic moment as a function of temperature and (c) critical current density, J_c, as a function of magnetic field for Ag-SmBCO processed with a Y-123 layer. The locations of the specimens within the parent single grain correspond to the positions illustrated in Figure 1 (c).

The characterisation methods used in the first part of this study (i.e for the Ag-SmBCO single grain processed without a Y-123 layer) were also performed on the Ag-SmBCO bulk superconductor processed with an additional Y-123 layer. Figure 6 shows the results of EPMA characterisation of this sample. The scales used in these figures are the same as those used for the equivalent results for the sample processed without a Y-123 layer, for ease of comparison.

The composition distribution along the *c*-axis measured by EMPA is shown in Figure 6 (a). The green solid lines are drawn to highlight the trends in the data. The sample fabricated with a Y-123 layer is expected to exhibit a more homogeneous distribution in composition along the *c*-axis with increasing distance from the seed [19]. Additional horizontal, solid green lines have been included in the figure in order to illustrate and compare the relative stability of the values of x and y in the

Ag-$Sm_xBa_yCu_3O_{7-\delta}$ superconducting bulk matrix. The concentrations of Sm and Ba in the Y-123, liquid-enriched sample are maintained with increasing distance from the seed, indicating a more homogeneous composition of $Sm_{1+x}Ba_{2-x}Cu_yO_z$ and a less severe substitution of Ba by Sm along the *c*-axis when the Y-123 layer is added, which is consistent with previous studies of the GdBCO system [19]. This represents the first observation of this effect in SmBCO bulk single grains processed in air.

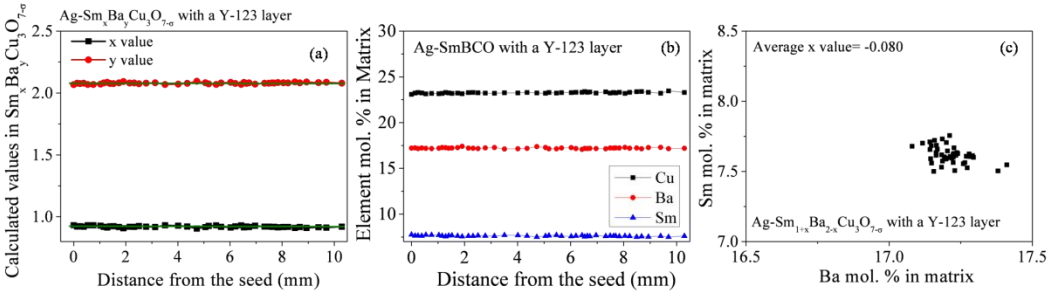

Figure 6 (a) Calculated values of x and y in Ag-SmBCO processed with a Y-123 layer with increasing distance from the seed along the *c*-axis, (b) Molar ratios of the elements of the Ag-SmBCO phase matrix fabricated with a Y-123 layer with increasing distance from the seed along the *c*-axis and (c) The concentration distribution of Sm and Ba in Ag-SmBCO fabricated with a Y-123 layer.

The homogeneity achieved by adding the Y-123 layer can be established by measurements of the superconducting properties, T_c and J_c, of the single grain along the *c*-axis from the position of the seed to the bottom of the composition-adjusted Ag-SmBCO sample, as shown in Figure 5 (b) and (c). The results of these measurements are related closely to the chemical composition of the Ag-SmBCO bulk superconducting sample and, unlike the results presented in Figures 3 (b) and (c),

those presented in Figure 5 (b) and (c) exhibit a significantly more homogeneous distribution throughout the parent single grain. This provides further evidence that the addition of a Y-123 layer enables effective adjustment of the composition of $Sm_{1+x}Ba_{2-x}Cu_yO_z$, resulting in a more uniform and consistent value of x along the *c*-axis in melt processed, single grain Ag-SmBCO, leading to almost identical J_c-B properties, which are sensitive to the microstructure of the sample.

Further microstructural studies have been performed on Ag-SmBCO single grains fabricated with and without a Y-123 layer in an attempt to observe the distribution of Sm-211 inclusions within the cross section of the Sm-123 matrix. Previous research concluded that $\boldsymbol{J_c}$ is determined by inhomogeneities in the sample microstructure, such as micro-cracks, RE-211 particle inclusions and twin planes [3]. Particularly, the particle size and distribution of RE-211 are directly correlated to $\boldsymbol{J_c}$ [20].To obtain complete information on the Sm-211 distribution, the present research examined the sample microstructure at intervals of 1 mm from the seed along the primary axes across the whole cross section. The selection of micrographs shown in Figure 7 form the basis of discussion of the effects of the Y-123 layer on the particle Sm-211 dispersion within the superconducting phase matrix. Figures 7 (a) and (b) show magnification at 500 × at a position under the seed and near the bottom of the Ag-SmBCO sample fabricated without a Y-123 layer. Figures 7 (c) and (d) show corresponding images for the Ag-SmBCO sample with a Y-123 layer. In the micrographs, the darker regions represent the Sm-211 particles in the Sm-123 matrix, whereas the larger bright spots indicate the presence of silver. The black regions are

pores in the matrix. It can be seen that more Sm-211 particles accumulate towards the bottom of the Ag-SmBCO fabricated without a Y-123 layer, whereas the degree of aggregation of Sm-211 particles in Ag-SmBCO fabricated with a Y-123 layer is much less severe. The more uniform distribution of Sm-211 particles is consistent with the observed homogeneous superconducting properties along the *c*-axis with increasing distance from the seed in Ag-SmBCO fabricated with a Y-123 layer.

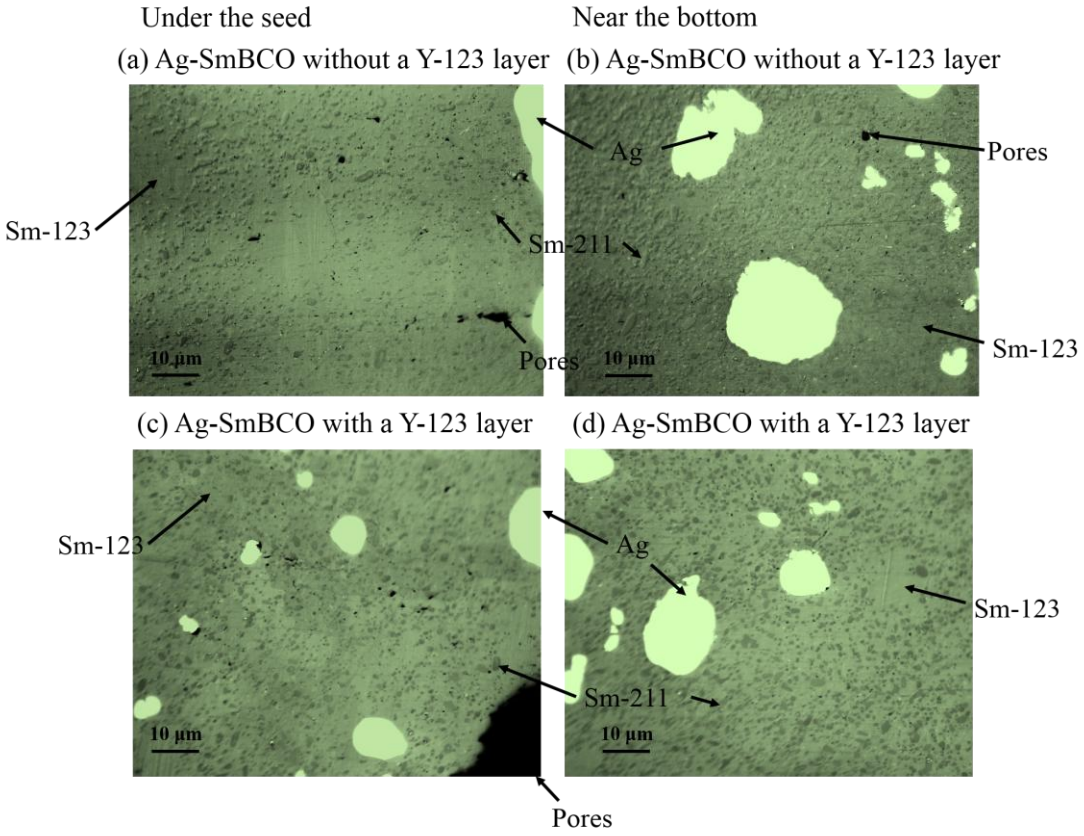

Figure 7 Micrographs at a magnification of 500 × for Ag-SmBCO fabricated without a Y-123 layer: (a) under the seed, (b) near the bottom of the sample; and Ag-SmBCO with a Y-123 layer: (c) under the seed, (d) near the bottom of the sample.

As indicated previously, only Sm and Ba require specific consideration when calculating x in the $Sm_{1+x}Ba_{2-x}Cu_yO_z$ superconducting phase formula, whereas the

amounts of Cu and O have been observed from EPMA measurements to be constant, as illustrated in Figure 6 (b).

The average value of x in $Sm_{1+x}Ba_{2-x}Cu_yO_z$, which was estimated from the data shown in Figure 6 (c), indicates that the value of x varies more gently for the single grain processed with a Y-123 layer, which indicates that the presence of a Y-123 layer is beneficial to processing a more uniform Ag-SmBCO bulk single grain. The value of x in $Sm_{1+x}Ba_{2-x}Cu_3O_{7-\delta}$ can be determined reliably, since the data collected are reasonably constant and their variation is within 1 mol. %, which is within the error of EPMA. The calculated average value of x is − 0.080 for samples grown with a Y-123 layer. This indicates that the substitution of Sm on the Ba site is enhanced by adding a Y-123 layer, which is due to the increase of the relative concentration of Sm ions in the liquid during TSMG. In addition, such enhanced Sm/Ba substitution accounts for the inferior irreversibility field and J_{c0} in Figure 5 (c).

4. Conclusions

In summary, we have reported for the first time that EPMA measurements can determine precisely the Sm/Ba substitution level in the Ag-SmBCO system fabricated in air. This method is even sensitive to subtle changes applied to the system, in the case in this study, by adding a Y-123 layer to the bottom of the bulk pre-form prior to melt processing in an attempt to provide a more homogenous Ag-SmBCO single grain with a controlled level of solid state substitution. The substitution levels of the Ag-SmBCO bulk single grains grown with and without a Y-123 layer have been measured, and demonstrate clearly that the substitution level of the Ag-SmBCO bulk

single grain grown without a Y-123 layer changes linearly with increasing distance from the seed. The value of x value measured for the composition-adjusted Ag-SmBCO bulk single grain, on the other hand, is relatively constant at -0.080, which suggests that Sm/Ba substitution for single grains processed in air can be detected accurately and controlled effectively. These results of this research have considerable potential for enabling further modification and development of the Ag-SmBCO system processed in air and optimisation of its superconducting properties, given that the level of Sm/Ba substitution determines critically these properties.

Acknowledgements

The authors acknowledge the financial support from the Engineering and Physical Sciences Research Council EP/P00962X/1. Additional data related to this publication are available at the University of Cambridge data repository (https://doi.org/10.17863/CAM.20841). The corresponding author would like to thank the financial support from the China Scholarship Council.

References

[1] R. Takahata, H. Ueyama, and A. Kubo, Characterization of Superconducting Magnetic Bearings (Runnout Performance at High Speed Rotation), in Advances in Superconductivity V: Proceedings of the 5th International Symposium on Superconductivity (ISS'92), November 16-19, 1992, Kobe, Y. Bando and H. Yamauchi, Eds. Tokyo: Springer Japan, 1993, pp. 1309-1312.

[2] Y. Miyagawa, H. Kameno, R. Takahata, and H. Ueyama, A 0.5 kWh Flywheel Energy Storage System using A High-T_c Superconducting Magnetic Bearing, IEEE Trans. Appl. Supercond., 9 (1999) 996-999.

[3] D. A. Cardwell, Processing and properties of large grain (RE)BCO, Mater. Sci. Eng., vol. B53, pp. 1-10, 1998.

[4] H. S. Chauhan and M. Murakami, Hot seeding for the growth of *c*-axis-oriented Nd-Ba-Cu-O, Supercond. Sci. Technol., 13 (2000) 672-675.

[5] N. H. Babu, Y. Shi, K. Iida, and D. A. Cardwell, A practical route for the fabrication of large single-crystal (RE)-Ba-Cu-O superconductors, Nat. Mater., 4 (2005) 476-480.

[6] S. Pinol, F. Sandiumenge, B. Martinez, V. Gomis, J. Fontcuberta, X. Obradors, E. Snoeck, and C. Roucau, Enhanced critical currents by CeO_2 additions in directionally solidified $YBa_2Cu_3O_7$, Appl. Phys. Lett., 65 (1994) 1448-1450.

[7] A. Goyal, P. D. Funkenbusch, D. M. Kroeger, and S. J. Burns, Fabrication of highly aligned $YBa_2Cu_3O_{7-\delta}$-Ag melt-textured composites, Phys. C, 182 (1991) 203-218.

[8] Y. Shi, N. Hari Babu, and D. A. Cardwell, Development of a generic seed crystal for the fabrication of large grain (RE)-Ba-Cu-O bulk superconductors, Supercond. Sci. Technol., 18 (2005) L13-L16.

[9] N. H. Babu, Y. Shi, K. Iida, and D. A. Cardwell, A practical route for the fabrication of large single-crystal (RE)-Ba-Cu-O superconductors, Nat. Mater.,

4 (2005) 476-480.

[10] W. Zhao, Y. Shi, A. R. Dennis, and D. A. Cardwell, Use of Sm- 123 + Sm- 211 Mixed-Powder Buffers to Assist the Growth of SmBCO and ZrO_2-doped SmBCO Single Grain, Bulk Superconductors, IEEE Trans. Appl. Supercond., 25 (2015) 6801305.

[11] W. Lo, D. A. Cardwell, and P. D. Hunneyball, Growth morphology of large YBCO grains fabricated by seeded peritectic solidification: (I) The seeding process, J. Mater. Res., 13 (1998) 2048-2056.

[12] W. Lo, D. A. Cardwell, C. D. Dewhurst, and S. L. Dung, Fabrication of large grain YBCO by seeded peritectic solidification, J. Mater. Res., 11 (1996) 786-794.

[13] D. X. Chen and R. B. Goldfarb, Kim model for magnetization of type-II superconductors, J. Appl. Phys., 66 (1989) 2489-2500.

[14] G. Krabbes, G. Fuchs, W. R. Canders, H. May, and R. Palka, High Temperature Superconductor Bulk Materials, Wiley-VCH Verlag GmbH & Co. KGaA, 2006.

[15] A. V. Narlikar, High Temperature Superconductivity 1: Materials, Springer Science & Business Media, 2004.

[16] N. Chikumoto, S. Ozawa, S. I. Yoo, N. Hayashi, and M. Murakami, Effects of oxygen content on the superconducting properties of melt-textured LRE123 superconductors, Phys. C Supercond., 278 (1997) 187-191.

[17] D. A. Cardwell and D. S. Ginley, Handbook of Superconducting Materials, second ed., vol. I, CRC Press, 2003.

[18] K. Iida, J. Yoshioka and M.Murakami, Superconducting properties of Nd-Ba-Cu-O fabricated in air, Physica C, 372-376 (2002) 1152-1154.

[19] D. Zhou, S. Hara, B. Li, J. Noudem, and M. Izumi, Flux pinning properties of Gd-Ba-Cu-O trapped field magnets grown by a modified top-seeded melt growth, Supercond. Sci. Technol., 27 (2014) 44015 (7 pp).

[20] M. Murakami, Processing of bulk YBaCuO, Supercond. Sci. Technol., 5 (1992) 185-203.